

Deconvoluting and Quantifying the Real-time Fluxes and Ionic Currents of Various Species Using *In Situ* Electrochemical Quartz Crystal Microbalance Measurements

Kai Zheng¹, Yongqiu Xian¹ and Zifeng Lin^{1,*}

¹College of Materials Science and Engineering, Sichuan University, Chengdu, 610065, Sichuan

*Corresponding Author E-mail Address: linzifeng@vip.163.com

Abstract

Electrochemical quartz crystal microbalance (EQCM) is a powerful technique to screen the gravimetric response of electrochemical electrodes. In this study, a straightforward mathematical method is proposed for extracting and deconvoluting the real-time fluxes and ionic currents of two species based on the EQCM measurement results. We creatively propose the concept of flux cyclic voltammograms (CVs) and ionic current CVs of various species and apply them to the real-time analyses of molecules/ions dynamics. For proof of concept, $\text{Ti}_3\text{C}_2\text{T}_x$ MXene, a most studied two-dimensional metal carbide, is investigated as a supercapacitor electrode in a 1M H_2SO_4 electrolyte. The H_2O and H^+ flux CV plots are highly symmetrical, indicating reversible inserting/deserting species fluxes. The highest fluxes along with maximum hydration numbers are obtained at the peak current potential. This suggests the significant contribution of double-layer capacitance originates from the insertion of hydrated H^+ . The H^+ CV with the ionic current induced by H^+ flux overlaps the real CV, confirming that H^+ is the only interactive ion for screening the electrode charge. Lastly, we also validate the proposed strategy using $\text{Ti}_3\text{C}_2\text{T}_x$ MXene electrode in 1M KCl electrolyte and YP80 porous carbon electrode in 1 M LiCl electrolyte.

Introduction

Quartz crystal microbalance (QCM) is a gravimetric probe based on the piezoelectric effect of a quartz resonator. By tracking the change of resonance frequency, the mass change of the resonance quartz can be calculated by employing the Sauerbrey equation.¹ This technique has been applied in the electro-deposition and dissolution of metal films, hydrogen absorption in

metals, under-potential deposition, and electrolyte adsorption, as well as with ion and solvent exchange in redox polymer layers and electrochemically driven self-assembly.²⁻⁶ Direct coupling of an electrochemical workstation with the QCM (EQCM) is used to measure the mass change of an electrode during electrochemical processes. This method is employed to determine the ions or solvent molecules insertion/desertion or electrode/electrolyte interphase formation.⁷⁻¹⁰ Levi *et al.* used the EQCM to measure the mass change in microporous carbon, to determine cation and anion insertion/desertion behavior.⁷ The solvation degree of ions within a selected potential range is typically estimated through the calculation of the average molecular weight per charge. This calculation is based on the slope of a linear regression function of the mass change (Δm) versus accumulated charge (Δq), as per Faraday's law of electrolysis.¹¹⁻¹² Tsai *et al.* investigated the average solvation number of 1-ethyl-3-methylimidazolium cations in acetonitrile in nanoporous carbon employing EQCM. Here the desolvation process was observed when cations were inserted into confined carbon pores.¹² In contrast to classical EQCM, ac-electrogravimetry coupled QCM and electrochemical impedance spectroscopy were developed to detect contributions from either charged or uncharged species, while separating the anionic, cationic, and free solvent contributions.¹³⁻¹⁵ In addition, EQCM with dissipation monitoring (EQCM-D) has been proposed to probe the viscoelastic and mechanical properties of electrodes.¹⁶⁻¹⁸

EQCM is an efficient tool to monitor real-time mass change. However, the population of charged species and/or solvent molecules, viscoelasticity or mechanical properties of electrodes, real-time solvation degree, or fluxes of various insertion/desertion species are often not accessible when EQCM is employed, or cannot be provided in full. Although some publications have reported the measurement of ionic fluxes using EQCM, only qualitative analysis or mass variation information was provided.^{7, 19-20} More importantly, deconvolution of real-time information of various species has not been achieved thus far. This would have important applications in several potential-dependent electrochemical processes, such as battery electrodes that store charge at redox potentials, or in monitoring the solvation variation versus potential. In these applications, the ability to monitor transient information of influx/efflux species would present a significant advantage, even more so than in applications

presented herein, where the average molecular weight or population change was monitored within a wide potential range.

Ti₃C₂T_x MXene with T_x stands for surface groups (such as -OH, -F, -O), is a two-dimensional transition metal carbide, which has been intensively investigated as a typical pseudocapacitive electrode material in acidic electrolytes²¹. The electrochemical signature of Ti₃C₂T_x MXene in H₂SO₄ electrolyte is featured with a pair of broad redox peaks in cyclic voltammetry (CV) plots.²² The pseudocapacitance originates from the redox reaction between inserted H⁺ and Ti₃C₂T_x MXene.²³ Our previous study has shown the insertion of hydrated H⁺ instead of bare H⁺, and the average molecular weight of the inserted species is 14 g mol⁻¹ according to the EQCM tests, corresponding to an average hydration number of 0.72.²⁴ The average hydration numbers of the inserted cations in the Ti₃C₂T_x MXene electrode have also been examined with several other neutral electrolytes.²⁵⁻²⁷ However, a full picture of H⁺ and H₂O flux dynamic is still lacking. In this study, the electrochemical process of Ti₃C₂T_x MXene in a 1M H₂SO₄ electrolyte was investigated. A mathematic method was applied to extract and deconvolute the real-time H₂O and H⁺ fluxes from EQCM measurement results. Fluxes CVs (*J*-CVs) of H₂O and H⁺ along with the H⁺ current CV were further constructed for better interpreting the charge storage behavior by direct observation on real-time and potential-dependent behavior of the H₂O and H⁺ dynamic.

Theoretical and method

The synthesis of MXene is described in the Supporting Information. During the QCM tests, the resonant resistance change (ΔR) and resonance frequency change (Δf) of the quartz crystals were recorded simultaneously. A low ΔR is typically required for establishing the gravimetric model, whereby Δf can be converted to mass change Δm according to the Sauerbrey's equation as follows.¹

$$\Delta m = -\frac{A\sqrt{\rho_q\mu_q}}{2f_0^2}\Delta f \quad (1)$$

where A , ρ_q , μ_q , and f_0 represents the area of the active piezoelectrical crystal (0.198 cm²), the density of quartz (2.65 g cm⁻³), the shear modulus of AT-cut quartz (2.947×10¹¹ g cm⁻¹ s⁻²), the base frequency (9.00 MHz), respectively. Based on the mass change Δm and accumulated

charge ΔQ , the average molecular weight M_w of the inserted species can be then calculated as follows.¹²

$$M_w = \left| \frac{\Delta m}{\Delta Q} \right| n F \quad (2)$$

where n and F represent the valence number of the charge carrier and Faraday constant (96485 C mol⁻¹), respectively. For a given electrode with i types of interactive species, the mass change Δm of the electrode would then be the sum of the masses of all inserted species, which can be expressed as

$$\Delta m = \Delta m_1 + \Delta m_2 + \cdots \Delta m_i \quad (3)$$

$$\Delta m = N_1 M_1 + N_2 M_2 + \cdots N_i M_i \quad (4)$$

Further, the corresponding accumulated charge can be calculated as

$$\Delta Q = -(\Delta q_1 + \Delta q_2 + \cdots \Delta q_i) \quad (5)$$

$$\Delta Q = -(N_1 x_1 + N_2 x_2 + \cdots N_i x_i) F \quad (6)$$

where Δm_i , Δq_i , N_i , M_i , and x_i , respectively, correspond to the mass change (g), charge (C), population (mol), molecular weight (g mol⁻¹) and valence number of the species that interact with the electrode during the electrochemical processes. Here, these species could be cations, anions, and/or solvent molecules, while, i is an integer that denotes i types of species. The charge values would be zero, positive, and negative for solvent molecules, cations, and anions, respectively. As both the charge accumulated at the electrode and ionic charge are opposite charge, thus a negative sign had to be incorporated in Equations (5) and (6).

Consequently, the mass and charge change at a specific time t (potential) can be expressed as

$$\Delta m_t = N_{1t} M_1 + N_{2t} M_2 + \cdots N_{it} M_i \quad (7)$$

$$\Delta Q_t = -(N_{1t} x_1 + N_{2t} x_2 + \cdots N_{it} x_i) F \quad (8)$$

Considering both the QCM and electrochemical workstation record data at specific intervals, results are presented as discrete data points. Assuming that S data points are collected throughout the measurement, over a period of t_s , while incorporating to Equations (7) and (8), the mass and charge changes at all time intervals are obtained using

$$\begin{bmatrix} \Delta m_{t_1} & \Delta m_{t_2} & \cdots & \Delta m_{t_s} \\ \Delta Q_{t_1} & \Delta Q_{t_2} & \cdots & \Delta Q_{t_s} \end{bmatrix} = \begin{bmatrix} M_1 & M_2 & \cdots & M_i \\ -x_1 F & -x_2 F & \cdots & -x_i F \end{bmatrix} \begin{bmatrix} N_{1t_1} & N_{1t_2} & \cdots & N_{1t_s} \\ N_{2t_1} & N_{2t_2} & \cdots & N_{2t_s} \\ \cdots & \cdots & \cdots & \cdots \\ N_{it_1} & N_{it_2} & \cdots & N_{it_s} \end{bmatrix} \quad (9)$$

Moreover,

$$A = \begin{bmatrix} \Delta m_{t_1} & \Delta m_{t_2} & \dots & \Delta m_{t_s} \\ \Delta Q_{t_1} & \Delta Q_{t_2} & \dots & \Delta Q_{t_s} \end{bmatrix} \quad (10)$$

$$B = \begin{bmatrix} M_1 & M_2 & \dots & M_i \\ -x_1 F & -x_2 F & \dots & -x_i F \end{bmatrix} \quad (11)$$

$$X = \begin{bmatrix} N_{1t_1} & N_{1t_2} & \dots & N_{1t_s} \\ N_{2t_1} & N_{2t_2} & \dots & N_{2t_s} \\ \dots & \dots & \dots & \dots \\ N_{it_1} & N_{it_2} & \dots & N_{it_s} \end{bmatrix} \quad (12)$$

where A is a matrix of mass (Δm_t) and charge (ΔQ_t) changes as function of time (t), obtained from the QCM and electrochemical measurements, and B is a matrix of the molecular weights (M_i) and valence numbers (x_i) of the different species. Finally, employing simple matrix calculations, X is a matrix of the population of the species (N_{it}) as a function of time (t). Furthermore, linear algebra would then dictate that the matrix X have a unique solution if $i \leq 2$. The proposed matrix computation method can therefore only be applied where no more than two interactive species are evaluated. Examples of this include scenarios where one type of ion species is coupled with one type of solvent, or where two ion species are considered. The practical applications would include capacitive electrodes operating in neat ionic liquid electrolytes and metal ion battery systems. In scenarios where three or more interactive species (i.e., anion, cation, and solvent) are to be evaluated, additional quantities would therefore have to be measured experimentally; this will not be discussed in this paper.

According to the real-time populations obtained from the matrix calculation, the species fluxes ($\frac{dN}{dt}$, denotes as J , nmol s⁻¹) can be obtained from the derivation of population versus time plots. However, the real-time population data from matrix X are presented as discrete data points that couldn't be used for derivative calculation. Therefore, plots of population versus time were fitted by fifth-order polynomials $F(t) = at^5 + bt^4 + ct^3 + dt^2 + et + f$ (a, b, c, d, e, f are constants to be determined by fitting, t is time) to achieve a continuous derivable function. Note that other continuous derivable functions that fit the data points well could be used. Thus, the molecular or ionic fluxes of any species i was given as

$$J(t)_i = \frac{dF(t)}{dt} \quad (13)$$

Following the determination of the real-time fluxes of various species during the CV scan, the flux cyclic voltammograms (J -CVs) could be plotted with flux and potential as Y and X-axis, respectively. Considering that the current ($\frac{dQ}{dt}$, A) of a measured CV is induced by the influx or efflux of charge carriers, the total global current can be deconvoluted into individual ionic

currents, corresponding to the ionic fluxes of the different species. The ionic current of the species i can be represented as follows

$$I_{ion_i} = \frac{dQ}{dt} = \frac{dN * F * (-x_i)}{dt} = J(t)_i * F * (-x_i) \quad (14)$$

Where x_i is the valance number of species i and F is the faradaic constant number. Thus, real-time ionic currents of all species can be calculated. Ionic current CVs can be plotted as well for interpreting the real-time current contributions of different species.

Finally, the population variation per potential ($\frac{dN}{dE}$, denoted as C_N ; nmol V⁻¹) was also calculated by dividing the molecular or ionic flux $J(t)$ with the scan rate v (Equation (15)). Moreover, the concept of population variation per potential is similar to the concept of capacitance ($\frac{dQ}{dE}$) in electrochemistry, which allows for the easy comparison of real-time population variation at different scan rates.

$$C_N(t) = J(t)/v \quad (15)$$

Results and discussion

Figure 1a shows the X-ray diffraction patterns of the Ti₃AlC₂ MAX phase and Ti₃C₂T_x MXene. Based on the chemical etching, the characteristic peaks of Ti₃AlC₂ disappeared, and the (002) peak shifted to a lower diffraction angle, indicating the successful synthesis of Ti₃C₂T_x MXene. The Ti₃C₂T_x MXene film was prepared via vacuum filtration, and transferred onto gold-coated quartz, and used as the working electrode in the EQCM cell (Figure S1).²⁶ The SEM image in Figure S1 shows a cross-section of the Ti₃C₂T_x MXene electrode film with an average thickness of approximately 200 nm. An appropriate thickness is required to ensure the gravimetric response, which in turn ensures that the resonance frequency shift can be calculated as the corresponding mass change by employing the Sauerbrey equation.^{16, 18} The electrochemical signature of Ti₃C₂T_x MXene was examined using a three-electrode Swagelok cell. The CV profiles in Figure S2 display a pair of broad and symmetric redox peaks within a stable potential window of -1.1 to -0.2 V vs Hg/Hg₂SO₄. These results are consistent with the previous results.²² For the EQCM measurements, a three-electrode EQCM cell (Figure S3) was assembled. Figure 1b presents the CV plot of the EQCM cell at 20 mV s⁻¹. Additionally, the potential window of

-0.95 to -0.2 V vs. Hg/Hg₂SO₄ was selected to avoid the irreversible hydrogen evolution reaction associated with the gold current collector. This selected potential range was still significantly larger than that employed in previous EQCM studies on Ti₃C₂T_x MXene in acidic electrolytes.^{24, 26} The results would therefore provide additional information on the charge storage mechanism in this expanded potential range. Meanwhile, the highly symmetrical CV profile (Figure 1b) at 20 mV s⁻¹ indicated excellent reversibility of the Ti₃C₂T_x MXene electrode with the negligible effect of background currents, and the CV shape over the selected potential range agreed well with those CVs obtained from the three-electrode Swagelok cell (Figure S2).

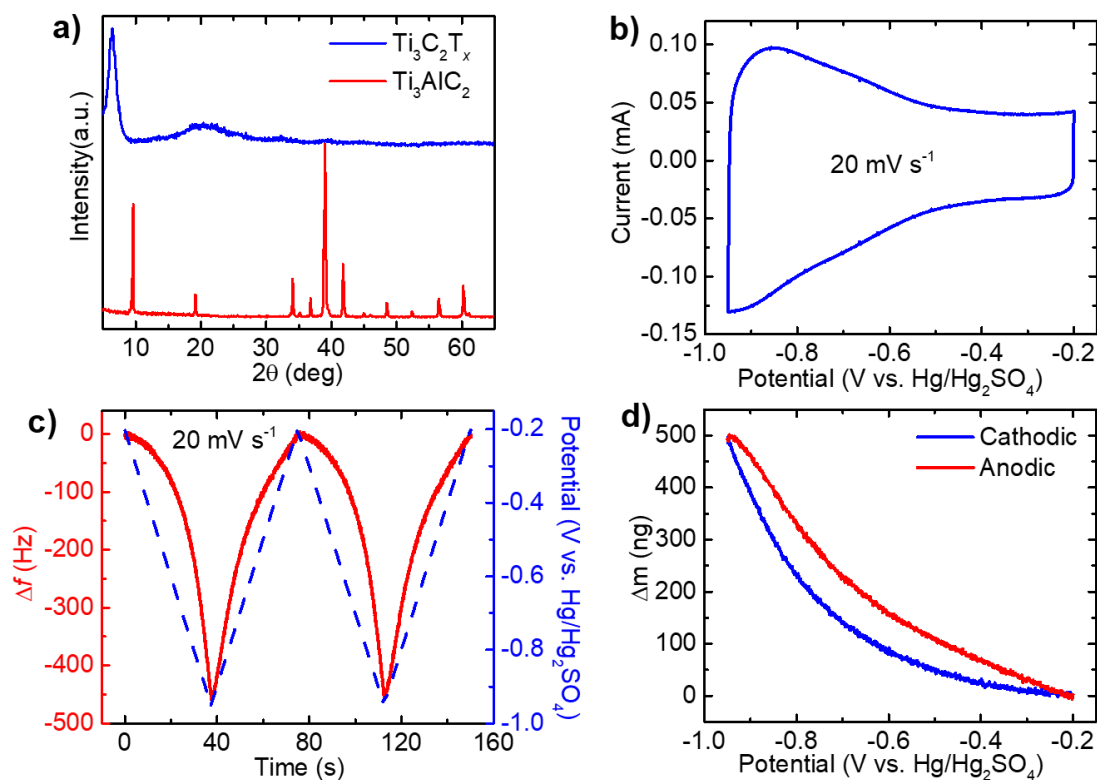


Figure 1. Material characterization and EQCM responses of the Ti₃C₂T_x MXene electrode in 1 M H₂SO₄ electrolyte at 20 mV s⁻¹. (a) XRD patterns of the Ti₃AlC₂ MAX phase and Ti₃C₂T_x MXene. (b) CV plot. (c) Resonance frequency change (Δf , Hz, red line) and potential evolution (V, blue dash line) versus time. (d) Mass change (Δm , ng) versus potential.

The validity of the rigid model of the QCM response is confirmed in Figure S4, where the

resonance resistance change (ΔR) is represented. The small variation observed ensure that the gravimetric model of the response can be described using the Sauerbrey's equation (Equation (1)). Figure 1c shows the QCM response versus time as determined during two CV cycles at 20 mV s⁻¹. The frequency change (Δf , Hz) agrees well with the evolution of the current versus potential, while exhibiting excellent reversibility. During the cathodic polarization, Δf gradually decreased from approximately 0 Hz at -0.2 V to a minimum value of approximately -470 Hz at -0.95 V. During the anodic scan, Δf returned to approximately 0 Hz, indicating a reversible process. According to Sauerbrey's equation, the decrease in the resonant frequency correlates with the mass increase of the electrode due to ions and/or solvent molecules interactions. The three possible interactive species that may be associate with 1 M H₂SO₄ electrolyte are H₂O, H⁺ and SO₄²⁻. Because the open circuit potential of the Ti₃C₂T_x MXene electrode is close to -0.2 V, negative polarization of the electrode will induce H⁺ insertion and/or SO₄²⁻ desertion. Considering that the molecular weight of SO₄²⁻ is 96 g mol⁻¹, which is significantly larger than those of H₂O (18 g mol⁻¹) and H⁺ (1 g mol⁻¹), the desertion of a substantial population of SO₄²⁻ will lead to a measurable mass decrease. However, according to Figure 1d, the electrode mass consistently increased during the full cathodic scan. And decreased reversibly during the anodic scan. This would indicate that SO₄²⁻ desertion/insertion during the cathodic/anodic process does not occur, which is consistent with previous results.²⁸ Figure 2a shows the mass change versus accumulated charge for the Ti₃C₂T_x MXene electrode during a complete CV cycle performed at 20 mV s⁻¹. As per convention, both the cathodic and anodic plots were divided into two regions, to distinguish between the slope changes at the intersection between regions I and II. The slopes were estimated from the individual linear regression functions fitted to the data, and determined according to Equation (2). During the cathodic process, the inserted species in region I were associated with an average molecular weight of 14.0 g mol⁻¹, consistent with previously reported result.²⁴ The average hydration number of 0.72 H₂O co-inserted per H⁺ in region I increased to 1.45 in region II. Moreover, the average molecular weight of the inserted species also increased to 27.1 g mol⁻¹. Conversely, for the anodic process, the average molecular weights were 18.2 (0.95 H₂O per H⁺) and 25.1 g mol⁻¹ (1.34 H₂O per H⁺) in region I and II, respectively. These results explain the small

differences observed between the charge storage kinetics of the cathodic and anodic processes, as well as the larger hydration numbers observed in region II. Owing to a lack of real-time hydration information, real-time changes in the hydration degree and ion migration are still not clearly understood.

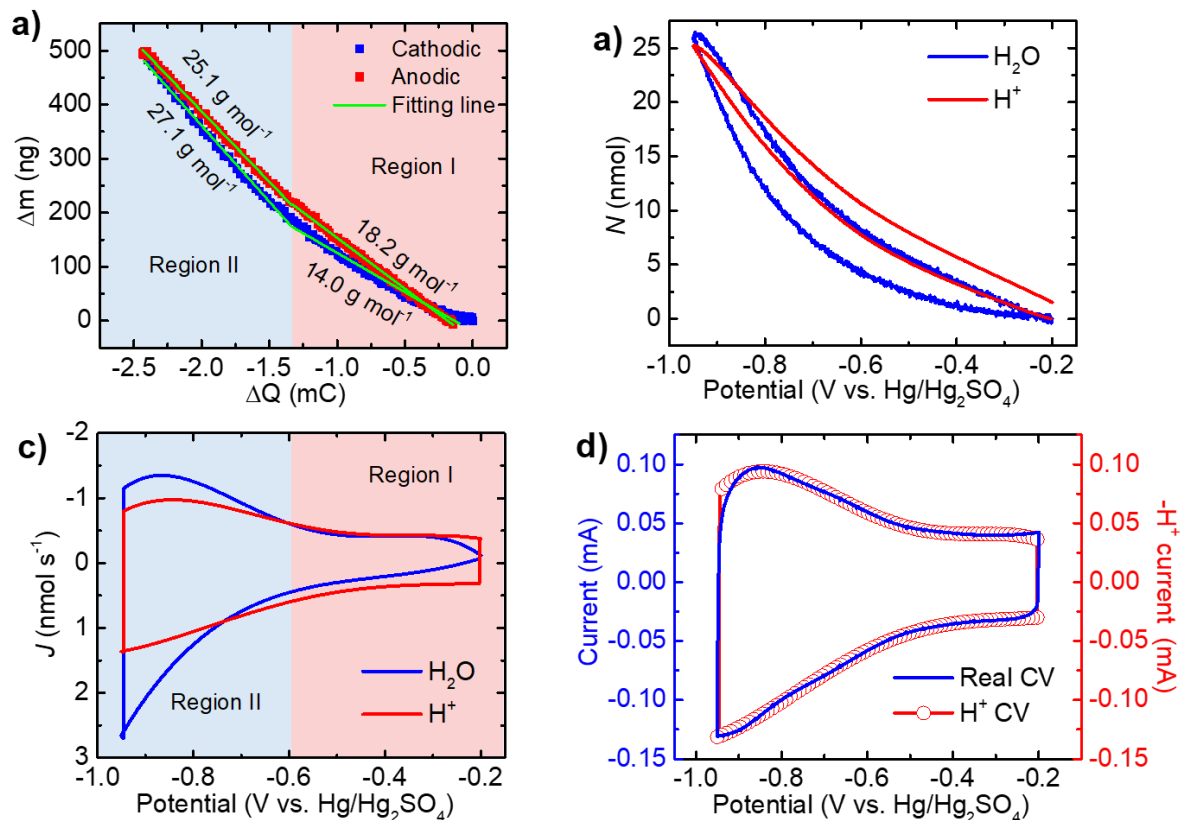


Figure 2. Analysis of EQCM data and real-time information during a full CV scan at 20 mV s^{-1} of $\text{Ti}_3\text{C}_2\text{T}_x$ MXene electrode in $1 \text{ M H}_2\text{SO}_4$ electrolyte. (a) Plots showing mass change (Δm , ng) versus accumulated charge (ΔQ , mC). Plot was divided into regions I and II to facilitate the fitting of a linear regression function. (b) Real-time population and (c) J -CVs of H_2O and H^+ . (d) H^+ CV (blue) and real CV (red).

To access the real-time information over the full potential domain, matrix computations were performed. As it has been discussed, only H_2O and H^+ (with valences of 0 and 1, respectively, and molecular weights of 18 and 1 g mol^{-1} , respectively) were considered as interactive species.

Equation (9) then becomes

$$\begin{bmatrix} \Delta m_{t_1} & \Delta m_{t_2} & \dots & \Delta m_{t_s} \\ \Delta Q_{t_1} & \Delta Q_{t_2} & \dots & \Delta Q_{t_s} \end{bmatrix} = \begin{bmatrix} 18 & 1 \\ 0 & -96485 \end{bmatrix} \begin{bmatrix} N_{\text{H}_2\text{O}t_1} & N_{\text{H}_2\text{O}t_2} & \dots & N_{\text{H}_2\text{O}t_s} \\ N_{\text{H}^+t_1} & N_{\text{H}^+t_2} & \dots & N_{\text{H}^+t_s} \end{bmatrix} \quad (16)$$

The mass change (Δm_t) and charge change (ΔQ_t) values in the matrix were obtained from the QCM and CV measurements. The real-time populations of H₂O ($N_{H_2O_t}$) and H⁺ ($N_{H^+_t}$) could thus be obtained by employing these matrix calculations.

The real-time populations (nmol) of H₂O and H⁺ were subsequently determined and plotted, as shown in Figure 2b. It can be seen that the population of H₂O increased during the cathodic scan, and decreased to approximately the starting value again during the anodic scan. This would imply the complete desorption of inserted H₂O. The population of H⁺ follows the same trend but does not completely return to zero. This could be explained by the irreversible charge contribution of the side reaction or leakage current. To obtain the real-time fluxes (nmol s⁻¹), real-time populations (nmol) of H₂O and H⁺ versus time were plotted and fitted by a continuous derivable function with all fitting goodness values R-Square >0.999 (Figure S5). Real-time fluxes (nmol s⁻¹) of H₂O and H⁺ could be achieved from the first derivative of $F(t)$ according to Equation (13) and plotted as flux CVs (J -CVs) in Figure 2c. The J -CVs were highly symmetrical, confirming the excellent reversibility of H₂O and H⁺ insertion/desorption. The J -CV of H⁺ exhibits a shape similar to the real CV curve, which could be expected as the charge at the Ti₃C₂T_xMXene electrode is screened only by H⁺. The H₂O flux exhibited a similar trend; an increasing flux was observed during the cathodic scan, and a decreasing flux was observed during the anodic scan. The real-time hydration number was calculated as the ratio of the H₂O to H⁺ fluxes, as shown in Figure S6. The hydration number further exhibited the same trend as observed with the response current, where an increase in the hydration number was associated with an increase in the response current. A maximum hydration number of approximately 2 was observed at the peak current potential. These results are noteworthy because the inserted hydrated cations may contribute significantly to the formation of an electric double layer (EDL).²⁹⁻³⁰ This EDL formation could explain the extremely high capacitance (approximately 375 F g⁻¹) observed for the Ti₃C₂T_xMXene electrode in acidic electrolytes, obtained previously. The results showed that approximately 60% of the total capacitance could be attributed to the redox reaction contribution. However, the limited specific surface area of the Ti₃C₂T_xMXene electrode would not be able to contribute the EDL capacitance, to account for the remaining 40% of the total capacitance.^{22, 24} Therefore, it can be concluded that the high capacitance of

Ti₃C₂T_x MXene electrode in the 1 M H₂SO₄ electrolyte is a combination of pseudocapacitance (charge transfer), surface EDL capacitance and interlayer EDL capacitance. Furthermore, the real-time molecular/ionic population and *J*-CVs at different scan rates were also calculated and presented in Figure S7. Interestingly, the maximum inserted populations of H₂O and H⁺, at 20, 50 and 100 mV s⁻¹ (Figure S7a and S7b) were similar; no apparent decrease could be identified at the high scan rates. This could therefore be considered indicative of the ultrafast kinetic of H₂O and H⁺ migration. Finally, the *J*-CVs of H₂O and H⁺ (Figure S7c and S7d) at 50 and 100 mV s⁻¹ were similar to those at 20 mV s⁻¹. According to Equation (14), the current contribution induced by the H⁺ flux is calculated and plotted as H⁺ CV. This calculated H⁺ CV coincided with the real CV (Figure 2d). It may therefore be concluded that H⁺ is the only species that accounts for the induced charge at the Ti₃C₂T_x MXene electrode. This concept of deconvoluting current into ionic currents, which were induced by different ion fluxes, could potentially also be successfully applied to electrochemical systems with two charge species. This would be particularly relevant as the electrochemical behaviors of various species are typically difficult to differentiate in these systems.

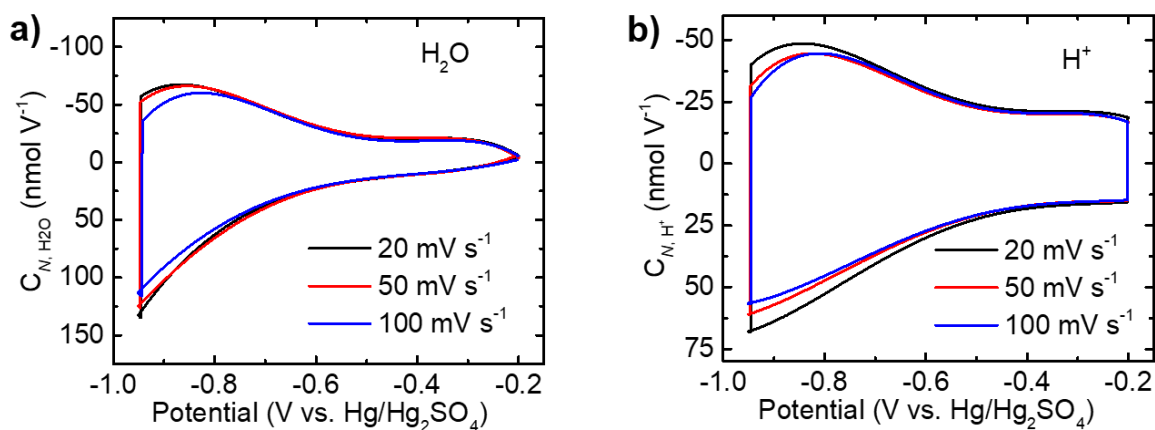


Figure 3. CVs of population variation versus potential (nmol V⁻¹) of Ti₃C₂T_x electrode in 1 M H₂SO₄ electrolyte. (a) H₂O and (b) H⁺ at 20, 50, 100 mV s⁻¹.

Furthermore, the variations of the H₂O and H⁺ populations versus voltage (nmol V⁻¹) at different scan rates were calculated according to Equation (15), as presented in Figure 3. Plots of the H₂O and H⁺ population changes per voltage at different scan rates overlapped at the high

potential range. This is indicative of a non-diffusion limitation associated with electrochemical double layer capacitive (EDLC) process. The decrease of H₂O and H⁺ population change versus voltage at low potential with increased scan rates could be explained by the inconsiderably slow kinetic of pseudocapacitive behavior as compared with the EDLC process at high potential range.

To verify the universality of the proposed method, Ti₃C₂T_x MXene electrode in 1 M KCl electrolyte and porous carbon YP80 electrode in 1 M LiCl electrolyte were also investigated. Figure 4a shows a rectangular CV plot of Ti₃C₂T_x coated quartz electrode in 1 M KCl electrolyte at 100 mV s⁻¹, which agrees well with the previous results.²⁵ Real-time populations of H₂O and K⁺ were obtained from the matrix computation method and plotted versus potential in Figure 4b. The H₂O population was much more than K⁺ population, indicating the higher hydrated degree of K⁺ as compared to H⁺. *J*-CVs of H₂O and K⁺ in Figure 4c confirm the higher H₂O flux than K⁺ flux at the full potential range. Hysteresis was observed for H₂O flux during the cathodic process, and the potential dependent hydration number was also reported elsewhere with Ti₃C₂T_x MXene electrode in LiCl aqueous electrolyte.^{25, 31} Converting the *J*-CV of K⁺ into corresponding K⁺ ionic current CV, it's found that the K⁺ CV overlapped well with the real CV, indicating K⁺ as the only charge carrier screens the electrode charge and Cl⁻ was not involved during the charge-discharge process. This conclusion was also confirmed by Shipgel et al that insertion of anionic species into MXene is not likely to occur²⁵. Similarly, electrochemical and real-time information of porous carbon YP80 electrode in 1 M LiCl electrolyte was provided in Figure S8. The potential-dependent hydration number was also confirmed. These results validate well the universality of the proposed method.

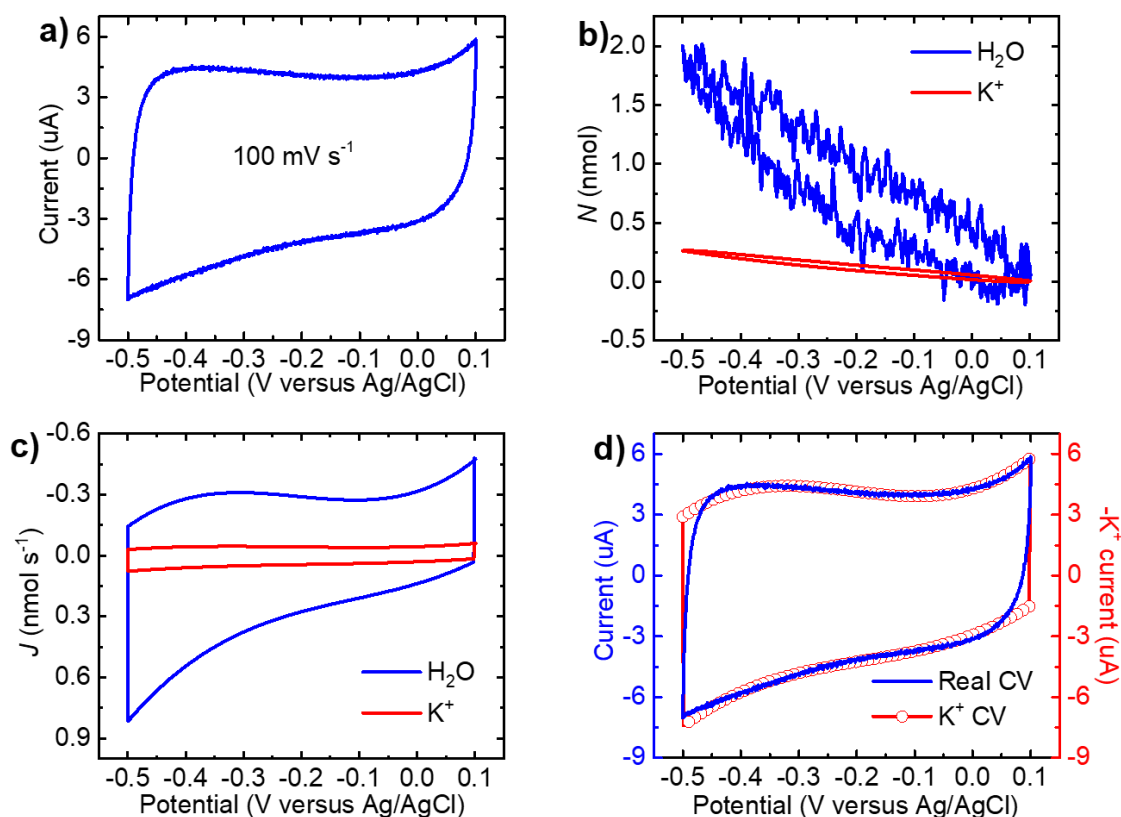


Figure 4. Electrochemical and EQCM characterizations of $\text{Ti}_3\text{C}_2\text{T}_x$ MXene electrode in 1 M KCl electrolyte at 100 mV s^{-1} . (a) Cyclic voltammetry plot. (b) Real-time population and (c) flux CVs (J -CVs) of H_2O and K^+ and (d) K^+ CV (blue) and real CV (red).

Conclusions

A straightforward mathematic strategy has been proposed for the construction and deconvolution of real-time flux CV and ionic current CV of different interactive species from EQCM measurement results. The proposed strategy was validated based on an investigation of $\text{Ti}_3\text{C}_2\text{T}_x$ MXene in a 1 M H_2SO_4 electrolyte. As part of this investigation, real-time H_2O and H^+ fluxes were determined and plotted as J -CV. The fluxes of both species exhibited similar trends as the CV current, where higher fluxes, with redox peaks, were obtained in the low potential range. The real-time hydration number exhibited similar behavior, with higher hydration numbers being obtained at potentials associated with a larger response current. These results suggest that the insertion of hydrated H^+ contributes significantly to EDL capacitance. Furthermore, the H^+ CV, as converted from the H^+ J -CV, agreed well with the experimentally determined CV, suggesting that H^+ is the only interactive charge carrier in this system. The

universality of the method is validated by investigations of $\text{Ti}_3\text{C}_2\text{T}_x$ MXene electrode in 1 M KCl electrolyte, as well as YP80 carbon electrode in 1M LiCl electrolyte. The concept of employing simple matrix computation to extract real-time information from electrochemical processes was introduced in this study. This approach enables the construction of flux and ionic current CVs for the interpretation of the real-time charge storage behavior of different ions, ultimately positioning the EQCM technique as a powerful tool for extensive application in various research fields.

Acknowledgments

This study was funded by the National Natural Science Foundation of China (Grant No. 52072252, No. 51902215), and Sichuan Science and Technology Program (No. 2020ZDZX0005), and the Fundamental Research Funds for the Central Universities (YJ201886).

References

1. Sauerbrey, G., Verwendung von Schwingquarzen zur Wägung dünner Schichten und zur Mikrowägung. *Z. Phys.* **1959**, *155* (2), 206-222.
2. Roto, R.; Rianjanu, A.; Rahmawati, A.; Fatyadi, I. A.; Yulianto, N.; Majid, N.; Syamsu, I.; Wasisto, H. S.; Triyana, K., Quartz Crystal Microbalances Functionalized with Citric Acid-Doped Polyvinyl Acetate Nanofibers for Ammonia Sensing. *ACS Applied Nano Materials* **2020**, *3* (6), 5687-5697.
3. Ho, C.-Y.; Wu, Y.-S., Diamine decorated graphene oxide film on quartz crystal microbalance for humidity-sensing analysis. *Applied Surface Science* **2020**, *510*, 145257.
4. Peugeot, A.; Creissen, C. E.; Karapinar, D.; Tran, H. N.; Schreiber, M.; Fontecave, M., Benchmarking of oxygen evolution catalysts on porous nickel supports. *Joule* **2021**, *5* (5), 1281-1300.
5. O'Sullivan, C. K.; Guilbault, G. G., Commercial quartz crystal microbalances – theory and applications. *Biosens. Bioelectron.* **1999**, *14* (8), 663-670.
6. Lin, Z.; Taberna, P.-L.; Simon, P., Advanced analytical techniques to characterize materials for electrochemical capacitors. *Current Opinion in Electrochemistry* **2018**, *9*, 18-25.
7. Levi, M. D.; Salitra, G.; Levy, N.; Aurbach, D.; Maier, J., Application of a quartz-crystal microbalance to measure ionic fluxes in microporous carbons for energy storage. *Nature Materials* **2009**, *8* (11), 872-875.
8. Yin, Z.-W.; Peng, X.-X.; Li, J.-T.; Shen, C.-H.; Deng, Y.-P.; Wu, Z.-G.; Zhang, T.; Zhang, Q.-B.; Mo, Y.-X.; Wang, K.; Huang, L.; Zheng, H.; Sun, S.-G., Revealing of the Activation Pathway and Cathode Electrolyte Interphase Evolution of Li-Rich

- 0.5Li₂MnO₃-0.5LiNi_{0.3}Co_{0.3}Mn_{0.4}O₂ Cathode by in Situ Electrochemical Quartz Crystal Microbalance. *ACS Appl. Mater. Interfaces* **2019**, *11* (17), 16214-16222.
9. Barisci, J. N.; Wallace, G. G.; Baughman, R. H., Electrochemical quartz crystal microbalance studies of single-wall carbon nanotubes in aqueous and non-aqueous solutions. *Electrochim. Acta* **2000**, *46* (4), 509-517.
 10. Liu, T.; Lin, L.; Bi, X.; Tian, L.; Yang, K.; Liu, J.; Li, M.; Chen, Z.; Lu, J.; Amine, K.; Xu, K.; Pan, F., In situ quantification of interphasial chemistry in Li-ion battery. *Nat. Nanotechnol.* **2019**, *14* (1), 50-56.
 11. Ye, J.; Wu, Y.-C.; Xu, K.; Ni, K.; Shu, N.; Taberna, P.-L.; Zhu, Y.; Simon, P., Charge Storage Mechanisms of Single Layer Graphene in Ionic Liquid. *Journal of the American Chemical Society* **2019**, *141* (42), 16559-16563.
 12. Tsai, W. Y.; Taberna, P. L.; Simon, P., Electrochemical quartz crystal microbalance (EQCM) study of ion dynamics in nanoporous carbons. *Journal of the American Chemical Society* **2014**, *136* (24), 8722-8728.
 13. Gao, W.; Krins, N.; Laberty-Robert, C.; Perrot, H.; Sel, O., Scrutiny of the LiCoO₂ Composite Electrode/Electrolyte Interface by Advanced Electrogravimetry and Implications for Aqueous Li-Ion Batteries. *The Journal of Physical Chemistry C* **2021**, *125* (7), 3859-3867.
 14. Arias, C. R.; Debiemme-Chouvy, C.; Gabrielli, C.; Laberty-Robert, C.; Pailleret, A.; Perrot, H.; Sel, O., New Insights into Pseudocapacitive Charge-Storage Mechanisms in Li-Birnessite Type MnO₂ Monitored by Fast Quartz Crystal Microbalance Methods. *The Journal of Physical Chemistry C* **2014**, *118* (46), 26551-26559.
 15. Lemaire, P.; Sel, O.; Alves Dalla Corte, D.; Iadecola, A.; Perrot, H.; Tarascon, J.-M., Elucidating the Origin of the Electrochemical Capacity in a Proton-Based Battery HxIrO₄ via Advanced Electrogravimetry. *ACS Appl. Mater. Interfaces* **2020**, *12* (4), 4510-4519.
 16. Shpigel, N.; Lukatskaya, M. R.; Sigalov, S.; Ren, C. E.; Nayak, P.; Levi, M. D.; Daikhin, L.; Aurbach, D.; Gogotsi, Y., In Situ Monitoring of Gravimetric and Viscoelastic Changes in 2D Intercalation Electrodes. *ACS Energy Letters* **2017**, *2* (6), 1407-1415.
 17. Shpigel, N.; Levi, M. D.; Sigalov, S.; Mathis, T. S.; Gogotsi, Y.; Aurbach, D., Direct Assessment of Nanoconfined Water in 2D Ti₃C₂ Electrode Interspaces by a Surface Acoustic Technique. *Journal of the American Chemical Society* **2018**, *140* (28), 8910-8917.
 18. Shpigel, N.; Levi, M. D.; Aurbach, D., EQCM-D technique for complex mechanical characterization of energy storage electrodes: Background and practical guide. *Energy Storage Materials* **2019**, *21*, 399-413.
 19. Sigalov, S.; Levi, M. D.; Salitra, G.; Aurbach, D.; Maier, J., EQCM as a unique tool for determination of ionic fluxes in microporous carbons as a function of surface charge distribution. *Electrochem. Commun.* **2010**, *12* (12), 1718-1721.
 20. Wu, Y.-C.; Taberna, P.-L.; Simon, P., Tracking ionic fluxes in porous carbon electrodes from aqueous electrolyte mixture at various pH. *Electrochem. Commun.* **2018**, *93*, 119-122.
 21. Lin, Z.; Shao, H.; Xu, K.; Taberna, P.-L.; Simon, P., MXenes as High-Rate Electrodes for Energy Storage. *Trends in Chemistry* **2020**, *2* (7), 654-664.
 22. Lukatskaya, M. R.; Kota, S.; Lin, Z.; Zhao, M.-Q.; Shpigel, N.; Levi, M. D.; Halim, J.; Taberna, P.-L.; Barsoum, M. W.; Simon, P.; Gogotsi, Y., Ultra-high-rate pseudocapacitive

- energy storage in two-dimensional transition metal carbides. *Nature Energy* **2017**, *2* (8), 17105.
23. Lukatskaya, M. R.; Bak, S.-M.; Yu, X.; Yang, X.-Q.; Barsoum, M. W.; Gogotsi, Y., Probing the Mechanism of High Capacitance in 2D Titanium Carbide Using In Situ X-Ray Absorption Spectroscopy. *Adv. Energy Mater.* **2015**, *5* (15), 1500589.
24. Shao, H.; Xu, K.; Wu, Y.-C.; Iadecola, A.; Liu, L.; Ma, H.; Qu, L.; Raymundo-Piñero, E.; Zhu, J.; Lin, Z.; Taberna, P.-L.; Simon, P., Unraveling the Charge Storage Mechanism of Ti₃C₂T_x MXene Electrode in Acidic Electrolyte. *ACS Energy Letters* **2020**, *5* (9), 2873-2880.
25. Shpigel, N.; Chakraborty, A.; Malchik, F.; Bergman, G.; Nimkar, A.; Gavriel, B.; Turgeman, M.; Hong, C. N.; Lukatskaya, M. R.; Levi, M. D.; Gogotsi, Y.; Major, D. T.; Aurbach, D., Can Anions Be Inserted into MXene? *Journal of the American Chemical Society* **2021**, *143* (32), 12552-12559.
26. Zhang, Q.; Levi, M. D.; Chai, Y.; Zhang, X.; Xiao, D.; Dou, Q.; Ma, P.; Ji, H.; Yan, X., Vacuum Filtration-and-Transfer Technique Helps Electrochemical Quartz Crystal Microbalance to Reveal Accurate Charge Storage in Supercapacitors. *Small Methods* **2019**, *3* (11), 1900246.
27. Muckley, E. S.; Naguib, M.; Wang, H.-W.; Vlcek, L.; Osti, N. C.; Sacci, R. L.; Sang, X.; Unocic, R. R.; Xie, Y.; Tyagi, M.; Mamontov, E.; Page, K. L.; Kent, P. R. C.; Nanda, J.; Ivanov, I. N., Multimodality of Structural, Electrical, and Gravimetric Responses of Intercalated MXenes to Water. *ACS Nano* **2017**, *11* (11), 11118-11126.
28. Lukatskaya, M. R.; Mashtalir, O.; Ren, C. E.; Dall'Agnese, Y.; Rozier, P.; Taberna, P. L.; Naguib, M.; Simon, P.; Barsoum, M. W.; Gogotsi, Y., Cation intercalation and high volumetric capacitance of two-dimensional titanium carbide. *Science* **2013**, *341* (6153), 1502-5.
29. Ando, Y.; Okubo, M.; Yamada, A.; Otani, M., Capacitive versus Pseudocapacitive Storage in MXene. *Advanced Functional Materials* **2020**, *30* (47), 2000820.
30. Boyd, S.; Ganeshan, K.; Tsai, W.-Y.; Wu, T.; Saeed, S.; Jiang, D.-e.; Balke, N.; van Duin, A. C. T.; Augustyn, V., Effects of interlayer confinement and hydration on capacitive charge storage in birnessite. *Nature Materials* **2021**, *20* (12), 1689-1694.
31. Wang, X.; Mathis, T. S.; Sun, Y.; Tsai, W.-Y.; Shpigel, N.; Shao, H.; Zhang, D.; Hantanasirisakul, K.; Malchik, F.; Balke, N.; Jiang, D.-e.; Simon, P.; Gogotsi, Y., Titanium Carbide MXene Shows an Electrochemical Anomaly in Water-in-Salt Electrolytes. *ACS Nano* **2021**, *15* (9), 15274-15284.

Supporting information for
Deconvoluting and Quantifying the Real-time Fluxes and Ionic Currents of
Various Species Using *In Situ* Electrochemical Quartz Crystal Microbalance
Measurements

Kai Zheng¹, Yongqiu Xian¹ and Zifeng Lin^{1,*}

¹College of Materials Science and Engineering, Sichuan University, Chengdu, 610065, Sichuan

*Corresponding Author E-mail Address: linzifeng@vip.163.com

Supplemental experimental details

Synthesis of Ti₃C₂T_x MXene

Ti₃C₂T_x MXene was synthesized according to the previously reported method.¹ 2 g Ti₃AlC₂ (11 Technology Co., Ltd.) was added into the mixture of 40 mL 9 M HCl (Chengdu Chron Chemical Co., Ltd) and 2 g LiF (aladdin). Subsequently, the mixture was constantly stirred magnetically in a water bath for 30 h at 40 °C. After etching, the obtained suspension was washed with deionized water and centrifuged at 3500 rpm for 10 min (L0-LX-H1850) several times, until the pH value reached around 6. To gain few-layer Ti₃C₂T_x flakes, the sediment was further delaminated by ultra-sonication for 20 min at 250 W (DS-1000Y), followed by fully deoxygenation by Ar flow.

Materials characterizations

X-ray diffraction patterns were recorded on a DX-2700 diffractometer using a Cu K α radiation (40 kV, 30 mA) with an X-ray wavelength (λ) of 1.542 Å at a step of 0.06 ° s⁻¹ over 2 θ range of 5°–65°. A scanning electron microscope (JSM 7900F, Japan) was used to observe the thickness and cross-section of Ti₃C₂T_x MXene film.

EQCM measurements

To prepare the MXene film electrode, 80 uL MXene suspension with a concentration of 5 mg mL⁻¹ was dispersed in 500 mL deionized water, then the MXene dilute solution was vacuum filtered through a cellulose microporous membrane. Subsequently, the MXene film coated on filter membrane was cut into 6 mm diameter pieces and attached to Ametek 5-mm-diameter Au-coated quartz crystal with the aid of PVDF binder (100 mg PVDF in 10 mL NMP). After transferring, the MXene-coated quartz electrode was

immersed into acetone for 40 min to fully dissolve the cellulose filter and then dried in a vacuum oven at 60 °C for overnight.

All the electrochemical measurements were conducted on the electrochemical workstation (Multi Autolab M204). Hg/Hg₂SO₄ reference electrode was used in 1 M H₂SO₄ solution and Ag/AgCl reference electrode was used in 1M KCl or LiCl electrolytes. Three-electrode Swagelok cell was assembled and tested at room temperature. The vacuum filtrated Ti₃C₂T_x MXene film served as the working electrode, two layers of GFA were used as the separators, and YP80 activated carbon electrode on Platine current collectors was used as the counter electrode. In situ QCM test was carried out with a three-electrode EQCM cell. Ti₃C₂T_x MXene film (or YP80 activated carbon film) coated on quartz sensor was used as the working electrode, and excessive (in capacity) graphite electrode was used as the counter electrode. The resonance frequency and resonance resistance were recorded by QCM 922A (Princeton Applied Research, America).

Supplemental Figures

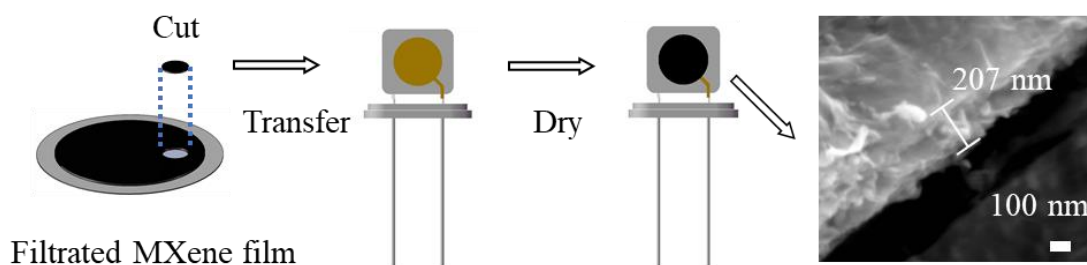


Figure S1. The diagram of Ti₃C₂T_x-coated quartz electrode preparation. Inset is the SEM image of Ti₃C₂T_x MXene film.

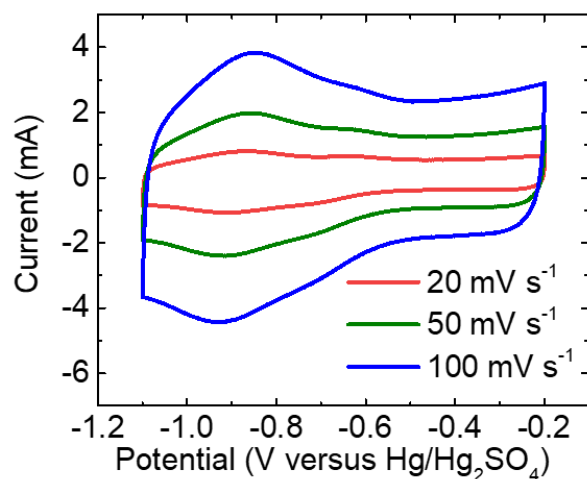


Figure S2. CV plots of a three-electrode Swagelok cell at scan rates from 20 mV s^{-1} to 100 mV s^{-1} within a potential window of 0.9 V.

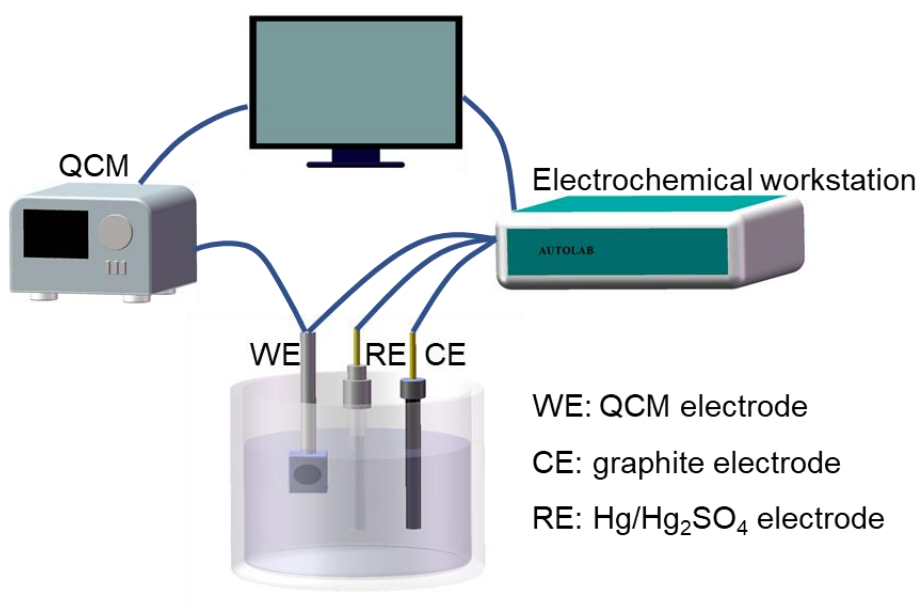


Figure S3. Scheme of three-electrode EQCM cell setup.

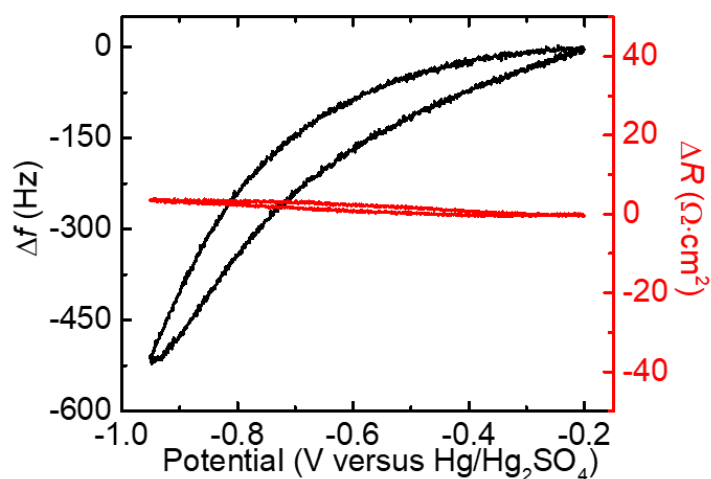


Figure S4. Plots of frequency change (Δf) and resonance resistance change (ΔR) vs. potential V after stabilization for $\text{Ti}_3\text{C}_2\text{T}_x$ -coated quartz electrode in 1 M H_2SO_4 at 20 mV s^{-1} .

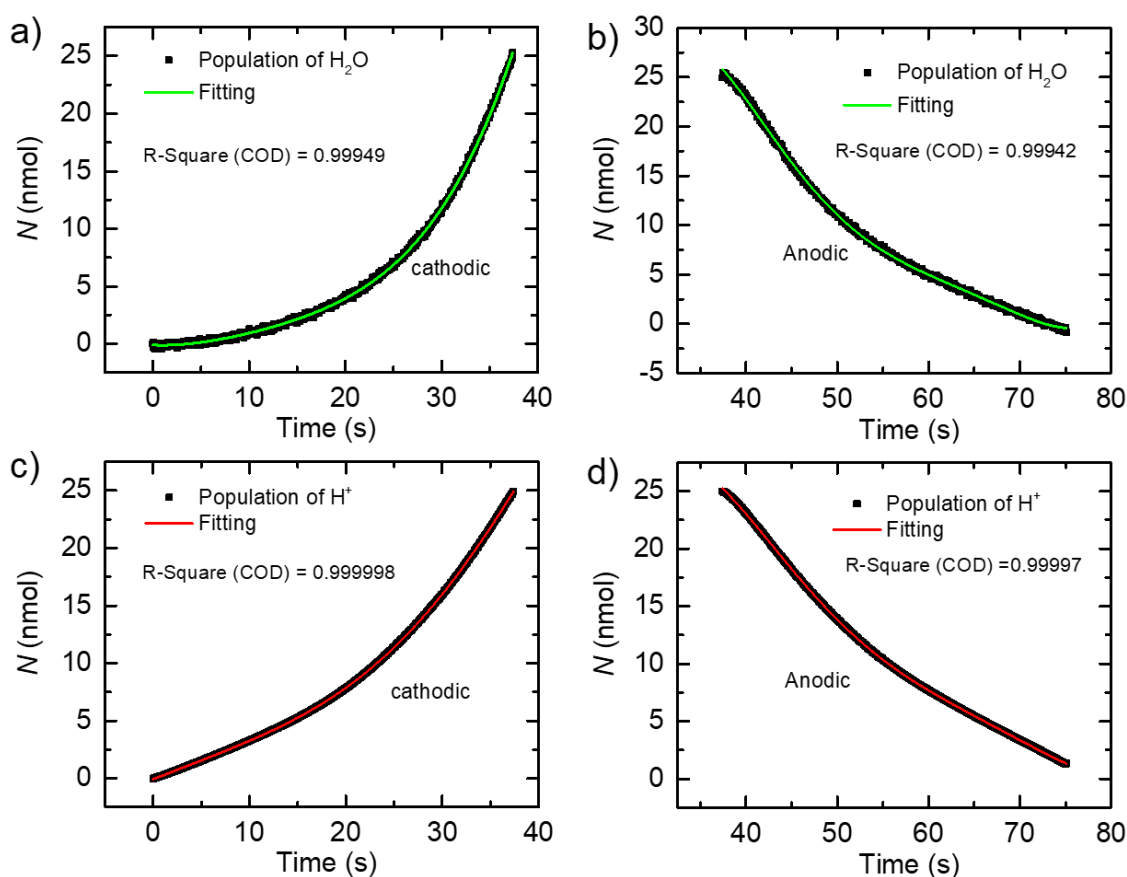


Figure S5. Plots of real-time H_2O and H^+ populations versus time during the CV scan at 20 mV s^{-1} and corresponding mathematic fitting by fifth-order polynomials $F(t)=at^5+bt^4+ct^3+dt^2+et+f$ (a, b, c, d, e, f are constants to be determined by fitting, t is

time). (a-b) H₂O information at (a) cathodic process, (b) anodic process. (c-d) H⁺ information at (c) cathodic process, (d) anodic process.

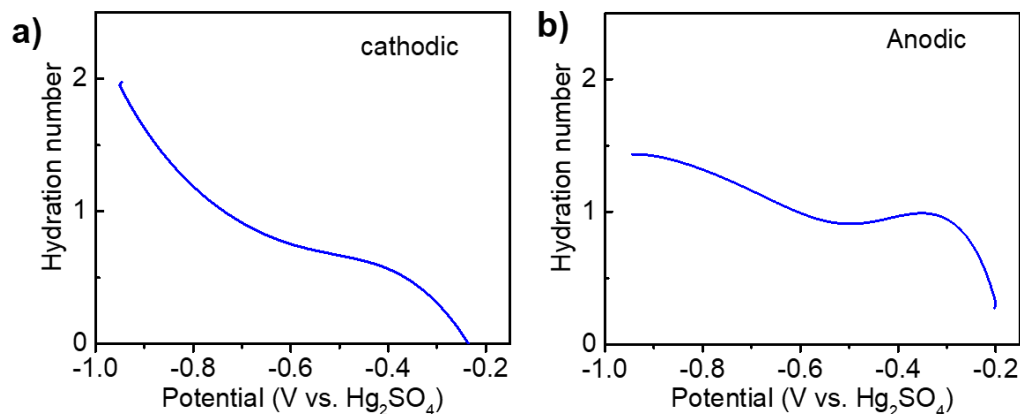


Figure S6. Real-time hydration number of inserting/deserting H⁺ during a full CV scan at 20 mV s⁻¹, (a) cathodic process, (b) anodic process.

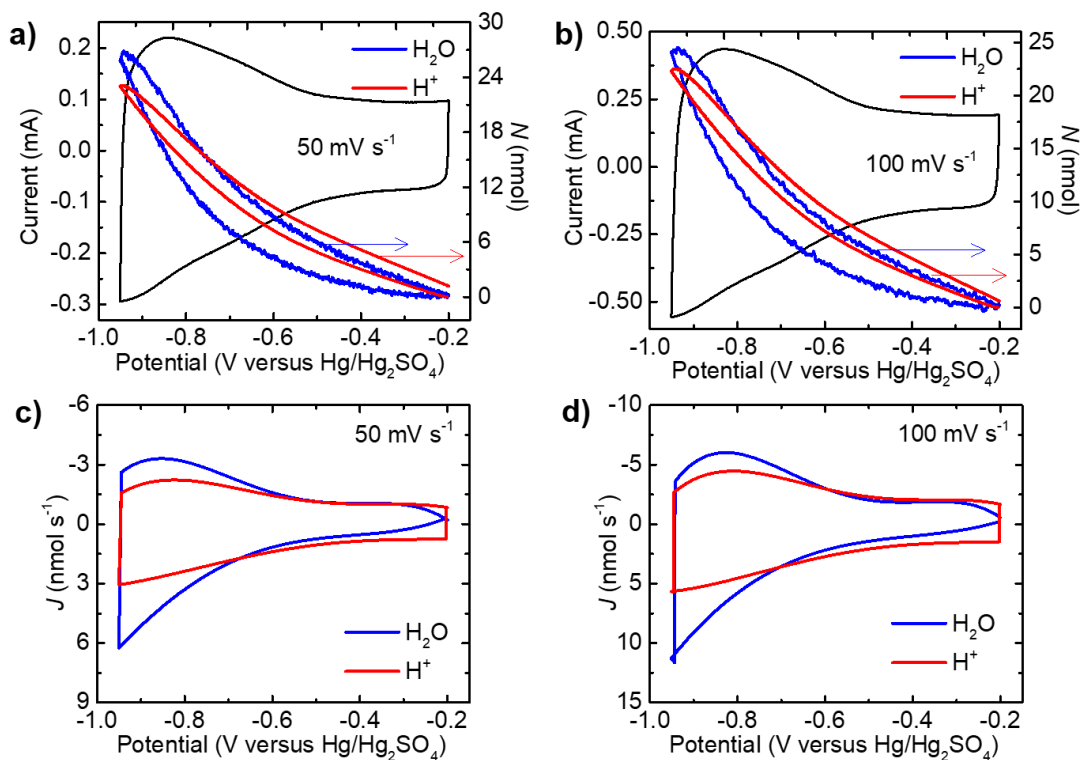


Figure S7. Real-time population of H₂O (blue) and H⁺ (red) and CV plots (black) of Ti₃C₂T_x MXene electrode at (a) 50 mV s⁻¹ and (b) 100 mV s⁻¹, and flux *J*-CVs of H₂O (blue) and H⁺ (red) at (c) 50 mV s⁻¹ and (d) 100 mV s⁻¹.

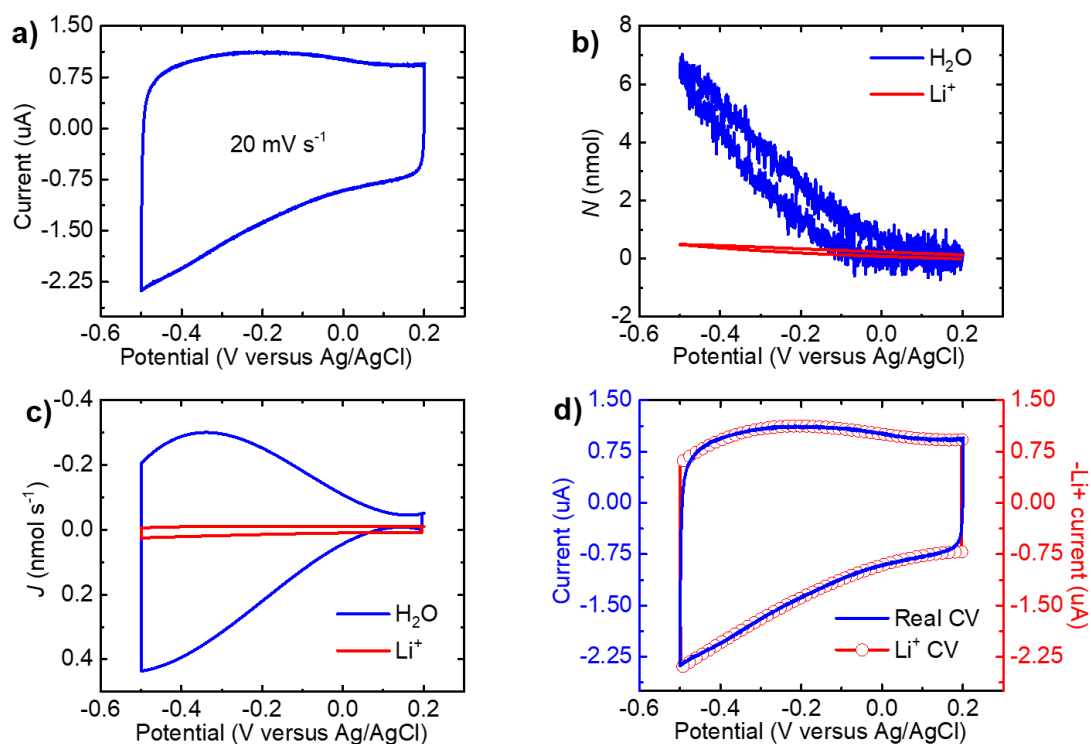


Figure S8. Electrochemical and EQCM characterizations of porous carbon electrode in 1 M LiCl electrolyte at 20 mV s⁻¹. (a) Cyclic voltammogram plot. (b) Real-time population and (c) flux CVs (*J*-CVs) of H₂O and Li⁺ and (d) Li⁺ CV (blue) and real CV (red).

Supplemental reference

1. M. R. Lukatskaya, S. Kota, Z. Lin, M.-Q. Zhao, N. Shpigel, M. D. Levi, J. Halim, P.-L. Taberna, M. W. Barsoum, P. Simon, and Y. Gogotsi, *Nature Energy*, **2** (8), 17105 (2017).